SCIENCE CHINA
Information Sciences

• Supplementary File •

Critical current for field-free switching of the in-plane magnetization in the three-terminal magnetic tunnel junction

Hongjie Ye[1†], Zhengjie Yan[1,3†], Min Wang[1] & Zhaohao Wang[1,2*]

[1]School of Integrated Circuit Science and Engineering, Beihang University, Beijing 100191, China
[2]National Key Lab of Spintronics, Institute of International Innovation, Beihang University, Hangzhou 311115, China
[3]Shen Yuan Honors College, Beihang University, Beijing 100191, China

Appendix A Details for theoretical derivation of the TST device

The Routh-Hurwitz criterion is a mathematical method used to determine the stability of a linear time-invariant (LTI) system by analyzing the roots distribution of their characteristic polynomial in the complex plane. Specifically, it checks whether all roots lie in the left half-plane (LHP), ensuring system stability, without explicitly solving for the roots. This method has been widely applied in various research fields, such as magnetodynamic [1], circuit stability assessment [2], and epidemiological disease spread prediction [3].

Based on the above criterion and LLG equation, two equilibriums $\vec{m} = (1, 0, 0)$ and $\vec{m} = (-1, 0, 0)$ are derived by setting $\partial \mathrm{m}_{x,y,z}/\partial t = 0$

$$H_d m_y m_z + H_{\mathrm{SOT}} m_x m_y - H_{\mathrm{STT}}(m_y^2 + m_z^2) = 0, \tag{A1}$$

$$-(H_d + H_k) m_x m_z - H_{\mathrm{SOT}}(m_x^2 + m_z^2) + H_{\mathrm{STT}} m_x m_y = 0, \tag{A2}$$

$$H_k m_x m_y + H_{\mathrm{SOT}} m_y m_z + H_{\mathrm{STT}} m_x m_z = 0, \tag{A3}$$

For the first formula, considering m_y and m_z are quite small, and H_d is much larger than H_{STT}, so Eq. (A1) can be rewritten as follows:

$$H_d m_y m_z + H_{\mathrm{SOT}} m_x m_y = 0, \tag{A4}$$

By combining Eq. (A3) and Eq. (A4), two equilibrium solutions are obtained, as:

$$E = \pm \left(m_x,\ \frac{H_{\mathrm{STT}} H_{\mathrm{SOT}} m_x}{H_d H_k - {H_{\mathrm{SOT}}}^2},\ -\frac{H_{\mathrm{SOT}} m_x}{H_d} \right), \tag{A5}$$

Next, by decoupling LLG equation, formulas for magnetization components along the x, y, and z directions are derived as:

$$\begin{cases} f_x = \dfrac{\gamma}{(1+\alpha^2)} \left\{ \alpha \left[H_k m_x (m_y^2 + m_z^2) + H_{\mathrm{SOT}} m_z + H_d m_x m_z^2 \right] - H_{\mathrm{STT}}(m_y^2 + m_z^2) + H_{\mathrm{SOT}} m_x m_y + H_d m_y m_z \right\}, \\ f_y = \dfrac{-\gamma}{(1+\alpha^2)} \left[\alpha \left(H_{\mathrm{STT}} m_z + H_k m_x^2 m_y - H_d m_y m_z^2 \right) + H_{\mathrm{SOT}}(m_x^2 + m_z^2) + H_k m_x m_z - H_{\mathrm{STT}} m_x m_y + H_d m_x m_z \right], \\ f_z = \dfrac{-\gamma}{(1+\alpha^2)} \Big[\alpha \left(H_{\mathrm{SOT}} m_x - H_{\mathrm{STT}} m_y + H_k m_x^2 m_z + H_d m_x^2 m_z + H_d m_y^2 m_z \right) \\ \qquad - H_{\mathrm{SOT}} m_y m_z - H_k m_x m_y - H_{\mathrm{STT}} m_x m_z \Big], \end{cases} \tag{A6}$$

The characteristic polynomial of the Jacobian matrix is written as:

$$P = a_0 \lambda^3 + a_1 \lambda^2 + a_2 \lambda + a_3, \tag{A7}$$

According to Routh-Hurwitz criterion, the critical condition for reaching equilibrium is that $\Delta_1, \Delta_2 > 0$, $a_0 > 0$ or when $\Delta_1, \Delta_2 < 0$, $a_0 < 0$. Here, Δ_1 and Δ_2 are given by:

$$\Delta_1 = a_1 = \frac{\gamma}{1+\alpha^2} \left[\alpha H_k (1 - 3m_x^2) + \alpha H_d (3m_z^2 - 1) + 2H_{\mathrm{SOT}} m_y + 2H_{\mathrm{STT}} m_x \right], \tag{A8}$$

* Corresponding author (email: zhaohao.wang@buaa.edu.cn)
† Hongjie Ye and Zhengjie Yan have the same contribution to this work.

$$\Delta_2 = \begin{Vmatrix} a_1 & a_0 \\ a_3 & a_2 \end{Vmatrix}, \tag{A9}$$

From the Jacobian matrix, it is easy to infer that $a_0 < 0$ in this case. Consequently, the equilibrium may become unstable under the condition $\Delta_1 > 0$, leading to magnetization switching. By substituting Eq. (A5) into $\Delta_1 > 0$ and considering $m_x \sim +1$, the switching condition can be derived as:

$$H_{\rm STT} > \alpha\left(1 - \frac{{H_{\rm SOT}}^2}{H_d H_k}\right)\left(H_k + \frac{{H_d}^2 - 3{H_{\rm SOT}}^2}{2H_d}\right), \tag{A10}$$

Finally, by incorporating both $H_{\rm STT}$ and $H_{\rm SOT}$:

$$H_{\rm STT} = \frac{\hbar P J_{\rm STT}}{2et_F M_s}, H_{\rm SOT} = \frac{\hbar\theta_{\rm SHE} J_{\rm SOT}}{2et_F M_s}, \tag{A11}$$

the critical switching current density for STT in the assistance of SOT is obtained as:

$$J_{\rm STT,c} = \frac{2\alpha e t_F M_s}{\hbar P}\left(1 - \frac{{H_{\rm SOT}}^2}{H_d H_k}\right)\left(H_k + \frac{{H_d}^2 - 3{H_{\rm SOT}}^2}{2H_d}\right), \tag{A12}$$

This formula is consistent with Eq. (3) in the main text, demonstrating an inverse correlation between $J_{\rm STT,c}$ and $J_{\rm SOT}$. The relationship has been experimentally corroborated [4, 5], confirming the validity of our model.

Appendix B Details for theoretical derivation of the canted Type-x device

Extending the above approach to the canted Type-x device, LLG equation can be further modified as:

$$\frac{\partial \vec{m}}{\partial t} = -\gamma \vec{m} \times \overrightarrow{H_{\rm eff}} + \alpha \vec{m} \times \frac{\partial \vec{m}}{\partial t} - \gamma H_{\rm SOT} \vec{m} \times (\vec{\sigma} \times \vec{m}), \tag{B1}$$

When the applied SOT current is canted from easy-axis, the spin polarization $\vec{\sigma}$ can be expressed as $(\sin\varphi, \cos\varphi, 0)$, where φ represents the canted angle, as shown in Figure 1(e) of the main text. Following the above approach, we get the formula of SOT critical switching current density:

$$J_{\rm SOT,c} = \frac{e t_F M_s}{\hbar\theta_{\rm SHE}} \frac{2H_d H_k \sin\varphi}{\alpha\,(2H_k + H_d)\cos^2\varphi} \times \left[\sqrt{1 + \frac{\alpha^2 (2H_k + H_d)^2 \cos^2\varphi}{H_d H_k \sin^2\varphi}} - 1\right], \tag{B2}$$

which is equivalent to Eq. (4) in the main text.

When considering the field-like torque (FLT), SOT is composed of two parts: damping-like torque (DLT) $\overrightarrow{\tau_{\rm DLT}} \propto \vec{m} \times (\vec{\sigma} \times \vec{m})$ and FLT $\overrightarrow{\tau_{\rm FLT}} \propto \vec{m} \times \vec{\sigma}$. In the Type-x device, the y-aligned spin-polarized current generates DLT, which drives magnetization to rotate towards the z-axis. The FLT exhibits characteristics of an in-plane bias field oriented along the hard-axis (y-direction), thus inducing magnetization deviation from equilibrium configuration while simultaneously reducing the energy barrier, contributing to the decrease in the switching current density [6]. However, in the case of large FLT/DLT ratio, FLT can also introduce additional degrees of freedom, leading to non-deterministic switching [7]. Therefore, the critical switching current cannot be well defined due to the oscillatory switching behavior.

Appendix C Details of simulation parameters

Main parameters in both macorspin and micromagnetic simulations are configured as follows: $\alpha = 0.033$, $M_s = 1000$ emu/cm^3, $\theta_{\rm SHE} = 0.3$ and $P = 0.6$. These values are basically consistent with the experimental measurements and simulation setups [8–10]. The initial magnetization state is defined as $m_x \sim +1$, and the complete switching is defined as $m_x \sim -0.9$ within 3 μs. The MTJ has an elliptical shape with a free layer thickness of 1.4 nm, and the aspect ratio is 2.

For macrospin simulations, $RK4$ algorithm with a step of 10^{-11} s is adopted. Micromagentic simulations are performed using the Object Oriented MicroMagnetic Framework (OOMMF) [11] and the exchange constant $A = 1.6\times10^{-11}$ J/m. Magnetic anisotropy is determined by saturation magnetization and the aspect ratio of the elliptical shape, which is calculated intrinsically by OOMMF. The mesh size is $2 \times 2 \times 1.4$ nm^3. For updating the magnetization configuration, we choose "Oxs_SpinXferEvolve" with a step size equal to 0.01 for the first candidate iteration and the $rk4$ method for Runge-Kutta implementation. Before the current is applied, the magnetization is set to relax for 1 ns. In addition, we set the stop-time of 3 μs in "Oxs_TimeDriver". All simulations are performed at zero temperature as the effect of thermal noise is not the focus of this work.

Appendix D Further analysis of the canted Type-x device

In the main text, Figure 1(f) illustrates the dependence of $J_{\rm SOT,c}$ on the canted angle φ. The relationship between $J_{\rm SOT,c}$ and φ follows an approximate proportion to $1/\sin\varphi$. The insets provide further details on magnetization dynamics under both critical and supercritical current conditions. As φ increases, the current required for switching decreases. Notably, the precession trajectory is shortened, indicating an accelerated switching response. Figure 1(g) shows the relative errors of Eq. (4) for different free layer dimensions. When the length of the main axis is less than 120 nm, the relative error remains within 1.25%. However, as the length increases to 160 nm, the relative error grows. This increase can arise from magnetic nucleation effects.

Further validation is conducted with the pulse-width-dependent switching measurements. The calculation of switching current density (J_{SOT}) is performed with various pulse width (t_{pulse}) followed by 5 ns relaxation. Therefore, the intrinsic SOT critical switching current density ($J_{\mathrm{SOT,c}}$) and the precession time (τ_0) can be extracted depending on the formula [12]

$$J_{\mathrm{SOT}} = J_{\mathrm{SOT,c}}\left(1 + \frac{\tau_0}{t_{\mathrm{pulse}}}\right), \tag{D1}$$

Figure D1(a) shows J_{SOT} as a function of φ in the range of $15 \sim 80$ deg with various t_{pulse} up to 8 ns. As φ increases, the SOT-driven switching dynamics transitions from an instability-dominated to a precession-dominated regime. In the long-pulse regime (t_{pulse}>1 ns), J_{SOT} decreases monotonically with increasing φ and eventually saturates, consistent with the prior report [13]. Notably, smaller φ values demonstrate a more gradual reduction of J_{SOT} with t_{pulse}, while larger φ display an accelerated decrease in current density. Therefore, J_{SOT} with φ=80 deg is even larger than that with φ=45 deg in the case of short-pulse (t_{pulse}<1 ns). This phenomenon has been reported by experimental work [14] and explained by the competition between the collinear and orthogonal components of spin accumulation [15].

In Type-y devices ($\varphi = 90$ deg), the initial magnetization is nearly parallel to $\vec{\sigma}$. Similarly to the case of $\varphi = 80$ deg, a minor angular deviation between the initial magnetization and $\vec{\sigma}$ results in a small but non-zero SOT strength (since SOT is proportional to $\vec{m} \times (\vec{\sigma} \times \vec{m})$). The collinear component dominates at larger φ, promoting precession-driven magnetization switching, whereas the orthogonal component enhances switching speed but necessitates higher J_{SOT} at smaller φ.

As shown in Figure D1(b), the slope of τ_0 at $\varphi = 80$ deg is steeper than that at smaller canted angles. This indicates that Type-y devices benefit from a longer precession time, which allows $\vec{m} \times \vec{\sigma}$ to have enough time for enhancement, resulting in a lower intrinsic switching current compared to Type-x devices. Moreover, $J_{\mathrm{SOT,c}}$ and τ_0 show the opposite trends with φ, intersecting at φ ~40 deg where both parameters reach relative minima. This intersection represents an experimentally favorable regime for balancing switching efficiency and energy consumption.

In Figure 1(h) of the main text, we obtained the critical SOT switching current density through two methods: general micromagnetic simulation and pulse-width-dependent switching measurement. Both of the two methods show a strong correlation with Eq. (4) after applying a scaling factor of k. The inset provides magnetization snapshots of the elliptical free layer, initialized with $m_x \sim +1$. Upon applying the current, the magnetization precesses along the y-axis, with the x-component gradually decreasing. Subsequently, the opposite magnetic domains form at both ends, leading to the fully switching within a short period of time.

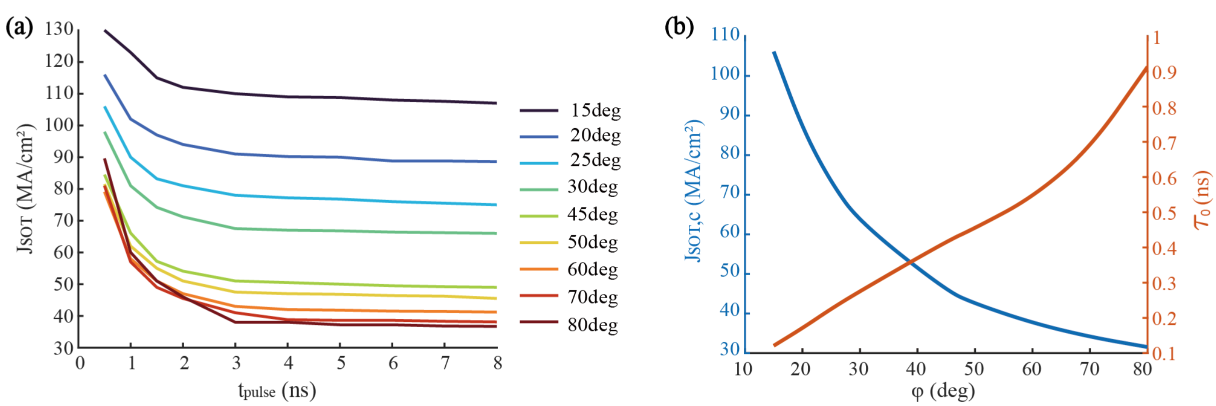

Figure D1 (a) SOT switching current density versus pulse width for different canted angles. (b) The critical switching current density and precession time for different canted angles.

References

1 Fano W G, Boggi S and Razzitte C A. Magnetic susceptibility of MnZn and NiZn soft ferrites using Laplace transform and the Routh–Hurwitz criterion. J Magn Magn Mater, 2011, 323: 1708–1711
2 Čermákn J and Nechvátal L. The Routh–Hurwitz conditions of fractional type in stability analysis of the Lorenz dynamical system. Nonlinear Dyn, 2017, 87: 939–954
3 Hassan T S, Elabbasy E M, Matouk A E, et al. Routh–Hurwitz Stability and Quasiperiodic Attractors in a Fractional-Order Model for Awareness Programs: Applications to COVID-19 Pandemic. Discrete Dyn Nat Soc, 2022, 1939260: 15
4 Zhang C, Takeuchi Y, Fukami S, et al. Field-free and sub-ns magnetization switching of magnetic tunnel junctions by combining spin-transfer torque and spin–orbit torque. Appl Phys Lett, 2021, 118: 9
5 Wang M, Cai W, Zhu D, et al. Field-free switching of a perpendicular magnetic tunnel junction through the interplay of spin–orbit and spin-transfer torques. Nat Electron, 2018, 1(11): 582–588
6 Fukami S, Anekawa T, Zhang C, et al. A spin–orbit torque switching scheme with collinear magnetic easy axis and current configuration. Nat Nanotechnol, 2016, 11: 621–625
7 Lee J M, Kwon J H, Ramaswamy R, et al. Oscillatory spin-orbit torque switching induced by field-like torques. Commun Phys, 2018, 1: 2

8 Taniguchi T, Isogami S, Shiokawa Y, et al. Magnetization switching probability in the dynamical switching regime driven by spin-transfer torque. Phys Rev B, 2022, 106: 104431

9 Zhang C, Fukami S, Watanabe K, et al. Critical role of W deposition condition on spin-orbit torque induced magnetization switching in nanoscale W/CoFeB/MgO. Appl Phys Lett, 2016, 109: 192408

10 Pathak S, Youm C, Hong J. Impact of Spin-Orbit Torque on Spin-Transfer Torque Switching in Magnetic Tunnel Junctions. Sci Rep, 2020, 10: 2799

11 Donahue M J, Porter D G: OOMMF User's Guide: Version 1.0. 1999

12 Liu Y T, Huang C C, Chen K H, et al. Anatomy of type-x spin-orbit-torque switching. Phys Rev Appl, 2021, 16: 024021

13 Fukami S, Anekawa A, Ohkawara A, et al. A sub-ns three-terminal spin-orbit torque induced switching device. In: Proceedings of IEEE Symposium on VLSI Technology, Honolulu, HI, USA, 2016. 1–2

14 Takahashi Y, Takeuchi Y, Zhang C L, et al. Spin-orbit torque-induced switching of in-plane magnetized elliptic nanodot arrays with various easy-axis directions measublack by differential planar Hall resistance. Appl Phys Lett, 2019, 114: 012410

15 Liu Y T, Huang Y H, Huang C C et al. Field-Free Type-x Spin-Orbit-Torque Switching by Easy-Axis Engineering. Phys Rev Appl, 2022, 18: 034019